Wastewater Treatment by Spiral Wound Reverse Osmosis: Development and Validation of a Two Dimensional Process Model

M. A. Al-Obaidi, C. Kara- Zaïtri and I. M. Mujtaba*

School of Engineering, Faculty of Engineering and Informatics. University of Bradford, Bradford, West Yorkshire BD7 1DP, UK

***Corresponding author, Tel.: +44 0 1274 233645**

E-mail address: I.M.Mujtaba@bradford.ac.uk

Abstract

Reverse osmosis (RO) has become a significant method for removing salts and organic compounds from seawater and wastewater in recent decades. Spiral-wound module has been widely used due to a number of special features such as high packing density, premium separation and low operating cost. In this paper, a two-dimensional mathematical model is developed for the transport of dilute aqueous solutions through a spiral-wound RO module and the operational characteristics of the process under steady state conditions are analysed. The model is based on the solution-diffusion model coupled with the concentration polarization mechanism. This model yields a set of Differential and Algebraic Equations (*DAEs*), which are solved using the *gPROMS* software. The model is validated using experimental data from the literature for the rejection of dimethylphenol as solute in aqueous solutions. The model is then used to simulate the process under steady state conditions to gain deeper insight of the process.

***Keywords*:** Wastewater Treatment; Reverse Osmosis; Two-Dimensional Process Model; Solution-diffusion Model.

1. Introduction

Reverse Osmosis (RO) is a pressure driven process used to remove salts/pollutants and purify water so, it can be used for various purposes such as human consumption, agricultural and industrial use (Sassi and Mujtaba, 2011). Spiral-wound membrane modules are often preferred in both desalination and industrial processes since it offers specific characteristics of accepted permeation rates, low energy requirements, low fouling levels, ease of operation and low water production costs (Evangelista, 1988). Generally, RO is considered as a less expensive technology in comparison with ultrafiltration (Chew et al., 2016). This technology also showed a dramatic growth for water recycling and wastewater treatment in several industries (Lee and Lueptow, 2001). For example, RO is widely considered for wastewater/effluent treatments in (a) textile industry (Amar et al., 2009) (b) dairy industry (Koyuncu et al., 2000; Álrez et al., 2002) (c) tannery industry (Bhattacharya et al., 2013) and (d) pharmaceutical industry (Mitra et al., 2012). These have stimulated continued research with an ultimate objective of maximizing the performance of the unit and reducing the cost of filtration with alleviation of environmental impact. For this purpose, a detailed but accurate process model is highly desirable, so that a reasonable prediction of the membrane performance can be obtained with feasible operating conditions for facilitating the best design of RO process.

There are a number of one and two-dimensional models in the literature developed to research the membrane performance of a spiral-wound module with different features and applications based on some assumptions and validated with sea and brackish water experimental data. Having said this, most of the suggested models have assumed constant pressure in a permeate channel (Karabelas et al., 2014). A critique on current literature is discussed in the following section.

A lumped model was developed by Gupta et al. (1985) for a spiral-wound module under laminar and turbulent flows and based on the solution-diffusion model. It presumes constant mass transfer coefficient and solute concentration at the feed channel and neglects solute concentration at the permeate channel.

Analytical models were developed by Rautenbach and Dahm (1987) for a spiral-wound module and worked out by Evangelista (1988), for high rejecting membranes and by Avlonits et al. (1991) and Boudinar et al. (1992) for both Roga and FilmTech membrane types respectively. These models considered the validity of the solution-diffusion model with a fully axial flow of brine solution and neglected the components of the tangential feed flow and the axial permeate flow. Also, these models assumed constant density and viscosity and ignored the concentration polarization impact. In addition to this, some of these models did not consider the pressure drop in the brine and permeate compartments.

Based on the three parameter model of the Spiegler and Kedem (1966), Senthilmurugan et al. (2005) and Mane et al. (2009) have developed models for turbulent flow by considering the pressure drop in both the channels. In comparison, Mane et al. (2009) have considered two dimensions (x and y) for the feed flow rate and stimulated the rejection of boron by the RO process.

Geraldes et al. (2005) have developed a one-dimensional model for spiral-wound RO membranes by ignoring both pressure drop in the permeate channel and the diffusion flow in the feed channel. While, Sagne et al. (2009) have considered a modified unsteady state one-dimensional model albeit by neglecting the concentration polarization impact and degrading the solute flux.

Avlonits et al. (2007) have developed a two-dimensional model by assuming only convective flux and neglecting diffusive mass transport and ignoring the variance of permeate concentration along the axial and spiral directions.

Oh et al. (2009) have developed a one-dimensional model based on the solution-diffusion model for spiral-wound RO system. It assumes constant mass transfer coefficient and constant water flux in the case of changing the inlet feed flow rate. Also, it neglects the pressure drop in the permeate channel. Kaghazchi et al. (2010) have proposed a one-dimensional model based on the solution-diffusion model where the bulk flow rate is calculated as an average value of inlet and outlet feed flow rates.

All the above models are validated with sea water and brackish water experimental data. In contrast, some comments on the proposed models that can be validated against wastewater treatment data are summarised in the next section.

A lumped model has been developed by Ahmad et al. (2007) for unsteady state simulation and validated with the experimental data of pre-treated palm oil mill effluent as a feed using a pilot plant scale RO system.

Sundaramoorthy et al. (2011a,b) have suggested a one-dimensional model by assuming the validity of the solution-diffusion model and constant values for both the permeate concentration and pressure along the permeate side. The model has been validated with the experimental data of chlorophenol and dimethylphenol solutes.

Fujioka et al. (2014) have also developed a one-dimensional model based on the irreversible thermodynamic model and considered the variety of the operating parameters by assuming zero permeate pressure. The model is validated against experimental data of N-nitrosamine rejection.

As can be seen from the above discussions that the models are restricted to one-dimension of spiral-wound RO process used especially for wastewater treatment and clearly neglect the tangential direction impact. Furthermore, Sundaramoorthy et al. 2011a confirmed that there

are only a few validation studies of mathematical models with wastewater experimental data. With the above backdrop, the initiative nature of this work lies in (a) the development of an explicit simple two-dimensional spiral-wound RO model applicable for dilute aqueous solution in wastewater treatment process (b) the validation of the model against experimental data from the literature and (c) the further application of the model to study the effect of various operating parameters on the performance of RO system. This model will be based on the solution-diffusion model and will relax the assumptions of constant physical properties, constant pressure and concentration of the fresh water on the permeate side considered in the past by many researchers. In addition, the brine concentration varies along the membrane length and width due to the impact of the plug-flow and diffusion flow. Also, it will consider the concentration polarization impacts on the whole unit.

2. Model development

2.1 The configuration of spiral-wound module

The configuration of the spiral-wound module essentially comprises a sealed envelope of membrane containing product water side and a spacer for the flowing of the feed. The membrane envelope is made of two sheets and sealed on three edges with an opening fourth edge connected with a central perforated pipe where the permeated water is collected. The narrow channels between the envelopes where the feed and permeate flow are filled with very thin fibers (spacers), which are wrapped around the permeated pipe. The dimensions of the used module can be shown in Table 1.

In most existing spiral-wound published models, the feed flow rate is in the axial direction while the permeate flow rate is in the spiral direction. However, it is supposed to account the impact of tangential feed flow rate and axial permeate flow rate within the mathematical model due to the promotion of turbulence caused by the existence of turbulence promoting

net. Also, using high pressures will make a substantial variation in the fluid mixing, mass transfer coefficient and pressure drop.

Fig. 1 depicts the spiral-wound module, which consists of two parts (the feed and permeate sides). The specific dimensions of the module are length and width L and W, where x is the coordinate along the membrane axial direction, and y is the coordinate in the spiral direction starting from the sealed end of the leaf to the end of membrane width. The feed and permeate spacers channels are t_f and t_p respectively with $(A_m = L\,W)$ as the area of the membrane. Also, according to the method of *dis-critization* used by *gPROMS* (Process system Enterprise Ltd., 2001), the area of the membrane will be split into 16 sub-sections of equal areas, where the proportion of each sub-section area will be obtained by:

$$A_{sub-section} = \Delta x\,\Delta y$$

Where, $\Delta x = \frac{L}{4}$ and $\Delta y = \frac{W}{4}$

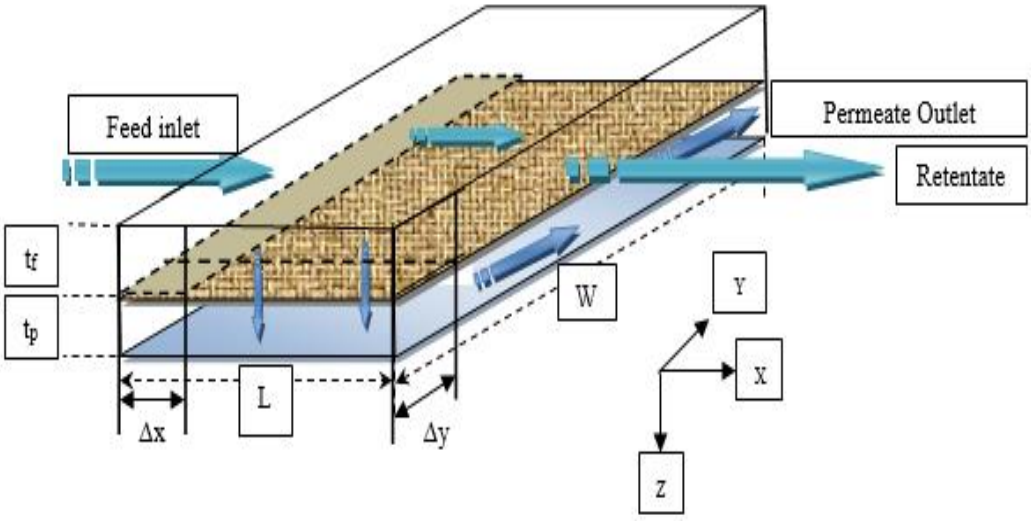

Fig. 1. Schematic diagram of the spiral-wound module

2.2 The main principles

The model will include the steady state equations in two-dimensions on both sides of the membrane for measuring the specific variables of the process at each point along the axial and tangential dimensions.

As mentioned above, this model will use the solution-diffusion model besides the concentration polarization theory to consider the variation of mass transfer coefficient in the feed channel. The validation of the model will be carried out using a case of wastewater treatment experimental data from the literature where dimethylphenol from diluted aqueous solutions was removed using a pilot scale spiral-wound module.

The procedure of the solution used in this model is by dividing the whole unit of the spiral-wound module to a number of equal individual sub-sections in two dimensions. Also, a guess for the initial value of permeate pressure (close to 1 atm) at the entrance of permeate channel will be considered to ensure 1 atm at the perforated pipe. Then, by using an analytical solution in *gPROMS*, the values of brine and permeate concentrations, wall concentration, brine and permeate pressures, temperatures, flow rates, water and solute fluxes will be calculated for each sub-section.

2.3 The assumptions

A number of reasonable assumptions and simplifications are used in order to develop this model:

1. The module is made up of a non-porous flat sheet with spacers and negligible leaf curvature.
2. Validity of the solution-diffusion model for the transport of the solvent and solute through the membrane.

3. Validity of the Darcy's law for the feed and permeate channels which assumes that the pressure drop is proportional to the feed and permeate flow rate in the case of laminar flow conditions and the friction parameter is applied to characterize the pressure drop.
4. Validity of the film model theory to estimate the concentration polarization impact.
5. The main value of the permeate concentration for all the increments will be taken as the total fresh water concentration since the flowing of outlet water is in the spiral direction towards the perforated collected pipe.

3. Model structure

To predict the characteristics of spiral-wound RO operation, the steady state mathematical model is suggested. From the above assumptions, the following sets of equations are formulated at any point in the system.

According to the solution-diffusion model, the characteristics of RO separation can be measured by the difference between the solvent and solute permeation fluxes J_w and J_s through the membrane.

The solvent flux $J_{w(x,y)}$ is proportional to the divergence between the hydraulic pressure difference and the osmotic pressure difference across the membrane by the construction:

$$J_{w(x,y)} = A_w \left(\Delta P_{b\,(x,y)} - \Delta\pi_{(x,y)}\right) \quad (1)$$

The solute flux $J_{s(x,y)}$ is calculated from the concentration difference across the two sides of the membrane (Lonsdale et al., 1965).

$$J_{s(x,y)} = B_s \left(C_{w(x,y)} - C_{p(x,y)}\right) \quad (2)$$

Where A_w and B_s are the pure water and solute permeability constants of the membrane respectively. Also, $\Delta P_{b(x,y)}$ is the trans-membrane pressure difference and $\Delta\pi_{(x,y)}$ is the osmotic pressure difference along the length and width of the membrane (L and W) defined

below by Eqs. (3) and (4). Also, $C_{w(x,y)}$ and $C_{p(x,y)}$ are the solute concentrations at the membrane wall and permeate side respectively.

$$\Delta P_{b\,(x,y)} = \left(P_{b(x,y)} - P_{p(x,y)}\right) \tag{3}$$

$$\Delta \pi_{(x,y)} = R\ T_{b(x,y)}\left(C_{w(x,y)} - C_{p(x,y)}\right) \tag{4}$$

Where R, $T_{b(x,y)}$, $P_{b(x,y)}$ and $P_{p(x,y)}$ are the gas constant, the temperature of the brine, the brine and the permeate pressures along the two dimensions of the unit respectively.

Since the solvent flux is much greater than the solute flux, the solute flux can be written as:

$$J_{s(x,y)} = J_{w(x,y)}\ C_{p(x,y)} \tag{5}$$

The accumulated impermeable solute on the membrane surface causes the concentration polarization layer and can be determined by using the stagnant film model proposed by Taniguchi (1978), by knowing the mass transfer coefficient, which depends on the axial and vertical motion of the solvent.

$$\left(\frac{J_{w(x,y)}}{k_{(x,y)}}\right) = \ln\left(\frac{C_{w(x,y)} - C_{p(x,y)}}{C_{b(x,y)} - C_{p(x,y)}}\right) \tag{6}$$

Where $k_{(x,y)}$ is the mass transfer coefficient for the back diffusion of the solute from the membrane to the bulk solution on high pressure side of the membrane along the two dimensions.

Substituting Eq. (4) in Eq. (1) yields:

$$J_{w(x,y)} = \left(A_w\left(\left(P_{b(x,y)} - P_{p(x,y)}\right) - R\ T_{b(x,y)}\left(C_{w(x,y)} - C_{p(x,y)}\right)\right)\right) \tag{7}$$

Also, re-arranging Eq. (7), gives.

$$J_{w(x,y)} = \frac{A_w\ \left(P_{b(x,y)} - P_{p(x,y)}\right)}{1 + \frac{C_{p(x,y)}\ R\ T_{b(x,y)}\ A_w}{B_s}} \tag{8}$$

Then, the solute fluxes and accumulated wall membrane concentration can be written as:

$$J_{s(x,y)} = \left(B_s\ exp\left(\frac{J_{w(x,y)}}{k_{(x,y)}}\right)\left(C_{b(x,y)} - C_{p(x,y)}\right)\right) \tag{9}$$

$$C_{w(x,y)} = \left(C_{p(x,y)} + exp\left(\frac{J_{w(x,y)}}{k_{(x,y)}}\right)\left(C_{b(x,y)} - C_{p(x,y)}\right)\right) \quad (10)$$

According to Darcy's law, the pressure drop in the brine and permeate channels along the membrane in two dimensions can be calculated from the momentum balance by considering the wall friction as the main cause of pressure drop as illustrated below:

$$\frac{dP_{b(x,y)}}{dx} + \frac{dP_{b(x,y)}}{dy} = -b\, F_{b(x,y)} \quad (11)$$

$$\frac{dP_{p(x,y)}}{dx} + \frac{dP_{p(x,y)}}{dy} = -b\, F_{p(x,y)} \quad (12)$$

Where b, $F_{b(x,y)}$ and $F_{p(x,y)}$ are the friction factor along the feed and permeate channels, the feed and permeate flow rates respectively.

From the sets of experimental data, the values of A_w, B_s and b can be calculated by using a graphical method proposed by Sundaramoorthy et al. (2011a).

For the purposes of accurate modeling, it is recommended to establish the momentum and material balance equations in the differential equations form for both the feed and permeate channels in two dimensions. This will interpret the variation of the specific variables of the unit, such as the brine and permeate concentrations.

Firstly, for the brine channel:

Combining Eq. (5) in Eq. (2) with arrangements, the permeate concentration in two dimensions can be calculated from Eq. (13) given below.

$$C_{p(x,y)} = \frac{C_{w(x,y)}}{\left(1+\frac{J_{w(x,y)}}{B_s}\right)} \quad (13)$$

The whole module mass balance equation can be derived as:

$$\frac{F_{b(0,y)}\,\rho_{b(o,y)}}{M_{wb}} = \frac{F_{b(x,y)}\,\rho_{b(x,y)}}{M_{wb}} + \frac{F_{p(x,y)}\,\rho_{b(x,y)}}{M_{wb}} \quad (14)$$

Where $F_{b(0,y)}$, $F_{b(x,y)}$, $F_{p(x,y)}$ and M_{wb} are the feed flow rate at the entrance of the unit, feed and permeate flow rates at any point on both feed and permeate channels and molecular weight of brine respectively.

By assuming a constant density and molecular weight, Eq. (14) can be re-written as:

$$F_{b(0,y)} = F_{b(x,y)} + F_{p(x,y)} \tag{15}$$

Also, the solute material balance is:

$$F_{b(0,y)}\, C_{b(0,y)} = F_{b(x,y)}\, C_{b(x,y)} + F_{p(x,y)}\, C_{p(x,y)} \tag{16}$$

The variation of the brine flow rate in both the x and y directions can be estimated from the solvent material balance:

$$\frac{d\left(\frac{F_{b(x,y)}}{\Delta x\ t_f}\right)}{dx} = -\left(\frac{J_{w(x,y)}}{t_f}\right) \quad \text{and} \quad \frac{d\left(\frac{F_{b(x,y)}}{\Delta y\ t_f}\right)}{dy} = -\left(\frac{J_{w(x,y)}}{t_f}\right) \tag{17}$$

Multiplying the above equations by ($\Delta x\ t_f$ and $\Delta y\ t_f$) respectively, yields:

$$\frac{dF_{b(x,y)}}{dx} = -\Delta x\, J_{w(x,y)} \quad \text{and} \quad \frac{dF_{b(x,y)}}{dy} = -\Delta y\, J_{w(x,y)} \tag{18}$$

Combining the above two equations to consider the two dimensions, yields:

$$\frac{dF_{b(x,y)}}{dx} + \frac{dF_{b(x,y)}}{dy} = -(\Delta x + \Delta y)\, J_{w(x,y)} \tag{19}$$

Similarly, the sub-section $(\Delta x, \Delta y)$ solute material balance equation in two dimensions can be formulated as below to express the brine concentration change at any point in the axial and vertical dimensions due to the impact of solute fluxes and diffusion terms.

$$\left[\left(\boldsymbol{F_{s(x)}\, t_f\, \Delta y}\right)_{\boldsymbol{x=0}} + \left(\boldsymbol{F_{s(x)} t_f\, \Delta x}\right)_{\boldsymbol{y=0}}\right] - \left[\left(\boldsymbol{F_{s(x)} t_f\, \Delta y}\right)_{\boldsymbol{x=\Delta x}} + \left(\boldsymbol{F_{s(y)} t_f\, \Delta x}\right)_{\boldsymbol{y=\Delta y}}\right] = \left(\boldsymbol{J_{s(x,y)}\, \Delta x\, \Delta y}\right) \tag{20}$$

Where $F_{s(x)}$ and $F_{s(y)}$ are the solute molar flux in the x and y directions defined in Eqs. (21) and (22).

$$F_{s(x)} = \frac{C_{b(x)}\, F_{b(x)}}{\Delta y\ t_f} - D_{b(x)} \frac{dC_{b(x)}}{dx} \tag{21}$$

$$F_{s(y)} = \frac{C_{b(y)}\, F_{b(y)}}{\Delta x\ t_f} - D_{b(y)} \frac{dC_{b(y)}}{dy} \tag{22}$$

Where $D_{b(x)}$ and $D_{b(y)}$ are the diffusivity coefficients of the brine in water in the x and y directions.

Dividing the two sides of Eq. (20) by the volume of sub-section ($t_f\, \Delta x\, \Delta y$) with an arrangement, it reduces to:

$$-\left[\frac{F_{s(x),\ x=\Delta x}-F_{s(x),\ x=0}}{\Delta x}\right]-\left[\frac{F_{s(y),\ y=\Delta y}-F_{s(y),\ y=0}}{\Delta y}\right]=\frac{J_{s(x,y)}}{t_f} \tag{23}$$

Again, it can be simplified.

$$\left[\frac{dF_{s(x)}}{\Delta x}\right]+\left[\frac{dF_{s(y)}}{\Delta y}\right]=-\frac{J_{s(x,y)}}{t_f} \tag{24}$$

Finally, combining Eqs. (21) and (22) in Eq. (24) with an arrangement, the equation of the brine concentration in two dimensions can be written as.

$$\frac{C_{b(x,y)}}{t_f.\Delta y}\frac{dF_{b(x,y)}}{dx}+\frac{F_{b(x,y)}}{t_f.\Delta y}\frac{dC_{b(x,y)}}{dx}+\frac{C_{b(x,y)}}{t_f.\Delta x}\frac{dF_{b(x,y)}}{dy}+\frac{F_{b(x,y)}}{t_f.\Delta x}\frac{dC_{b(x,y)}}{dy}=\frac{d}{dx}\left[D_{b(x,y)}\frac{dC_{b(x,y)}}{dx}\right]+\frac{d}{dy}\left[D_{b(x,y)}\frac{dC_{b(x,y)}}{dy}\right]-\frac{J_{s(x,y)}}{t_f} \tag{25}$$

Eq. (25) can be simplified.

$$\frac{d\frac{\left(C_{b(x,y)}F_{b(x,y)}\right)}{t_f\,\Delta y}}{dx}+\frac{d\frac{\left(C_{b(x,y)}F_{b(x,y)}\right)}{t_f\,\Delta x}}{dy}=-\frac{J_{s(x,y)}}{t_f}+\frac{d}{dx}\left(D_{b(x,y)}\frac{dC_{b(x,y)}}{dx}\right)+\frac{d}{dy}\left(D_{b(x,y)}\frac{dC_{b(x,y)}}{dy}\right) \tag{26}$$

The brine temperature equation (with assuming constant heat capacity for both brine and permeate) can be written as.

$$\left[\frac{F_{b(x,y)}\left(T_{b(x-1,y)}-T_{b(x,y)}\right)}{t_f\,\Delta x\,\Delta y}\right]=\left[\frac{J_{w(x,y)}\left(T_{b(x,y)}-T_{p(x,y)}\right)}{t_f}\right] \tag{27}$$

Similar expressions for the permeate channel are obtained as mentioned bellow:

$$\frac{C_{p(x,y)}}{t_f.\Delta y}\frac{dF_{p(x,y)}}{dx}+\frac{F_{p(x,y)}}{t_f.\Delta y}\frac{dC_{p(x,y)}}{dx}-\frac{d}{dx}\left[D_{p(x,y)}\frac{dC_{p(x,y)}}{dx}\right]+\frac{C_{p(x,y)}}{t_f.\Delta x}\frac{dF_{p(x,y)}}{dy}+\frac{F_{p(x,y)}}{t_f.\Delta x}\frac{dC_{p(x,y)}}{dy}-\frac{d}{dy}\left[D_{p(x,y)}\frac{dC_{p(x,y)}}{dy}\right]=\frac{J_{s(x,y)}}{t_f} \tag{28}$$

$$\left(\frac{dF_{p(x,y)}}{dx}\right)+\left(\frac{dF_{p(x,y)}}{dy}\right)=(\Delta x+\Delta y)\,J_{w(x,y)} \tag{29}$$

$$0=\left[\frac{J_{w(x,y)}\left(T_{b(x,y)}-T_{p(x,y)}\right)}{t_f}\right] \tag{30}$$

Where T_b and T_p are the temperature of the brine and permeate channels respectively.

Also, the accumulation of permeate flow rate for each sub-section (Δx and Δy) can be composed in the contour of Eq. (31).

$$F_{p(x,y)}=J_{w(x,y)}\,\Delta x\,\Delta y \tag{31}$$

%total water recovery $\mathrm{Rec}_{(\mathrm{Total})}$ and %solute rejection $\mathrm{Rej}_{(\mathrm{av})}$ can be written as (Srinivasan et al., 2011).

$$Rec_{(Total)} = \frac{F_{p(Total)}}{F_{b(0,y)}}\ x100 \quad (32)$$

$$F_{p(Total)} = \sum F_{p(x,y)} \qquad \text{From } (0,0) \text{ to } (L,W) \quad (33)$$

$$Rej_{(av)} = \frac{C_{b(x=L,y)} - C_{p(av)}}{C_{b(x=L,y)}}\ x100 \quad (34)$$

$$C_{p(av)} = \sum C_{p(x,y)} \qquad \text{From } (0,0) \text{ to } (L,W) \quad (35)$$

Where $C_{b(x=L,y)}$, $C_{p(av)}$ and $F_{p(Total)}$ are the outlet brine concentration, average permeate concentrations and the total permeated flow rate respectively.

3.1 The physical properties equations

This study covers the experimental work of dilute dimethylphenol aqueous solutions on spiral-wound module, so the physical properties equations of the solution has been conceived as identical to water equations (Koroneos et al., 2007). The mass transfer coefficient in the high pressure channel of the module depends on the solution properties, such as viscosity, solute diffusivity and the hydrodynamic conditions in the channel which is a function of pressure, concentration, flow rate and temperature. It means that k will vary with the membrane length and width.

The mass transfer coefficient of dimethylphenol at the feed channel can be calculated from.

$$k_{(x,y)}\ de_b = 246.9\ D_{b(x,y)}\ Re_{b(x,y)}^{0.101}\ \ Re_{p(x,y)}^{0.803}\ \ C_{m(x,y)}^{0.129} \quad (36)$$

Where the exponents in the above equation have been experimentally predicted by Srinivasan et al. (2011) for dimethylphenol aqueous solutions. Also, C_m is a dimensionless solute concentration and can be found from:

$$C_{m(x,y)} = \frac{C_{b(x,y)}}{\rho_w} \quad (37)$$

Where ρ_w is the molal density of water (55.56 kmol/m³).

The Reynolds number on the feed and permeate channels can be calculated from:

$$Re_{b(x,y)} = \frac{\rho_{b(x,y)}\ de_b\ F_{b(x,y)}}{t_f\ W\ \mu_{b(x,y)}} \quad (38)$$

$$Re_{p(x,y)} = \frac{\rho_{p(x,y)}\ de_p\ J_{w(x,y)}}{\mu_{p(x,y)}} \quad (39)$$

Where de_b and de_p are the equivalent diameters of the feed and permeate channels respectively.

$$de_b = 2t_f \quad \text{and} \quad de_p = 2t_p \quad (40)$$

4. Results and discussion

4.1 Model parameter estimation

The parameters of the model will be estimated by using the proposed graphical method of linear fit of Sundaramoorthy et al. (2011a). This method will be used to determine the values of solvent transport coefficient A_w, solute transport coefficient B_s and the feed channel friction parameter b. The details of these parameters are mentioned in Table 1. The estimated values of solvent transport parameters and solute transport parameters showed some difference than the values suggested by Srinivasan et al. (2011).

4.2 Steady state simulation

A commercial thin film composite RO membrane packed into a spiral-wound module (Make: Ion Exchange, India Ltd.) is used by Srinivasan et al. (2011) in their experimental work to remove a solute of dimethylphenol from aqueous solutions of different concentrations. The characteristics of the spiral-wound module are presented in Table 1. The solute concentrations of dimethylphenol varied from 0.819E-3 to 6.548E-3 kmol/m³. The feed was pumped at three different flow rates of 2.166E-4, 2.33E-4 and 2.583E-4 m³/s with a set of inlet feed pressures varied from 5.83 to 13.58 atm for each flow rate.

In the simulation study, the experimental data will be used to predict the best values of unknown parameters, which then used with the known parameters to check the behavior of the unit with the variety of operating variables.

Table 1: Input data: Membrane characteristics and geometry

Make	Ion Exchange, India Ltd. [a]
Membrane material	TFC Polyamide
Module configuration	Spiral-wound
Feed spacer thickness (t_f)	0.8 *mm*
Permeate channel thickness (t_p)	0.5 *mm*
Module length (L)	0.934 *m*
Module width (W)	8.4 *m*
Module diameter	3.25 *inches*
b	9400.9 $\left(\frac{atm\ s}{m^4}\right)$
A_w	9.42009E-7 $\left(\frac{m}{atm\ s}\right)$
B_s (dimethylphenol)	2.22577E-8 $\left(\frac{m}{s}\right)$

[a]: Manufacturer

4.2.1 Model validation

For aqueous solutions of dimethylphenol, Tables 2 to 4 depict the experimental results of Srinivasan et al. (2011) and the model predictions for three groups of feed flow rates; (each group holding five different feed concentrations under five different feed pressures) with estimating percentage of error between the experimental and the model predictions.

Tables 2 to 4 compare the experimental and the model prediction for the outlet brine concentration, outlet brine pressure, outlet feed flow rate, average permeate concentration and average solute rejection with a lot of different inlet feed flow rates, pressures and concentrations.

Table 2

Model validation with experimental results for inlet feed flow rate of ($F_{b(0,y)}$ =2.166E-4 m^3/s)

				Pb(outlet), (atm)			Cb(outlet)x10^3 (kmol/m^3)			Cp(av.)x10^3 (kmol/m^3)			Rej(av)			Fb(outlet)x10^4 (m^3/s)		
No	Pb (inlet) (atm)	Tb (inlet) (°C)	Cb(inlet) x10^3 (kmol/m^3)	Exp.	The.	%Error	Exp.	The.	%Error	Exp.	The.	%Error	Exp.	The.	%Error	Exp.	The.	%Error
1	5.83	32.5	0.819	4.46	4.06	8.96	0.9500	0.9230	2.84	0.0931	0.0885	4.84	0.902	0.904	-0.22	1.8	1.916	-6.44
2	7.77	32.5	0.819	6.31	6.06	3.96	1.0164	0.9909	2.51	0.0864	0.0734	15.0	0.915	0.9259	-1.19	1.67	1.786	-6.94
3	9.71	32.5	0.819	8.14	8.06	0.98	1.0821	1.0710	1.03	0.0790	0.0662	16.2	0.927	0.9382	-1.20	1.59	1.656	-4.15
4	11.64	32.5	0.819	9.98	10.05	-0.70	1.1562	1.1650	-0.75	0.0740	0.0623	15.8	0.936	0.9466	-1.13	1.5	1.528	-1.86
5	13.58	32.5	0.819	11.8	12.05	-2.11	1.2568	1.2800	-1.83	0.0729	0.0600	17.6	0.942	0.9531	-1.17	1.37	1.399	-2.11
6	5.83	31	1.637	4.41	4.05	8.16	1.8839	1.8300	2.86	0.1526	0.1730	-13.3	0.919	0.9051	1.51	1.851	1.932	-4.37
7	7.77	31	1.637	6.27	6.05	3.50	2.0227	1.9580	3.20	0.1335	0.1405	-5.24	0.934	0.9276	0.68	1.736	1.807	-4.08
8	9.71	31	1.637	8.09	8.05	0.49	2.1210	2.1100	0.52	0.1209	0.1272	-5.21	0.943	0.9397	0.34	1.63	1.681	-3.12
9	11.64	31	1.637	9.93	10.03	-1.00	2.2882	2.2830	0.22	0.1167	0.1189	-1.88	0.949	0.9479	0.11	1.523	1.557	-2.23
10	13.58	31	1.637	11.76	12.03	-2.29	2.4255	2.4940	-2.82	0.1140	0.1140	0.00	0.953	0.9543	-0.13	1.416	1.433	-1.20
11	5.83	31	2.455	4.37	4.042	7.50	2.7989	2.7310	2.42	0.2575	0.2367	8.07	0.908	0.9133	-0.58	1.868	1.942	-3.96
12	7.77	31	2.455	6.22	6.038	2.92	2.9783	2.9170	2.06	0.2204	0.1900	13.7	0.926	0.9348	-0.95	1.761	1.819	-3.29
13	9.71	31	2.455	8.05	8.034	0.19	3.1192	3.1350	-0.50	0.1778	0.1680	5.51	0.943	0.9464	-0.36	1.666	1.696	-1.80
14	11.64	31	2.455	9.89	10.02	-1.31	3.3529	3.3880	-1.04	0.1710	0.1557	8.94	0.949	0.954	-0.52	1.566	1.576	-0.63
15	13.58	31	2.455	11.72	12.016	-2.52	3.5062	3.6900	-5.24	0.1683	0.1482	11.9	0.952	0.9598	-0.81	1.478	1.453	1.69
16	5.83	30	4.092	4.32	4.03	6.71	4.6600	4.5070	3.28	0.3029	0.2730	9.87	0.935	0.9393	-0.45	1.898	1.962	-3.37
17	7.77	30	4.092	6.17	6.024	2.36	4.8066	4.7870	0.40	0.2884	0.3130	-8.52	0.94	0.9344	0.59	1.808	1.848	-2.21
18	9.71	30	4.092	8	8.017	-0.21	5.1470	5.1160	0.60	0.2625	0.2740	-4.38	0.949	0.9467	0.24	1.681	1.731	-2.97
19	11.64	30	4.092	9.84	10	-1.62	5.2933	5.4950	-3.80	0.2382	0.2525	-6.00	0.955	0.954	0.10	1.65	1.617	2.00
20	13.58	30	4.092	11.67	11.99	-2.74	5.6648	5.9410	-4.87	0.2096	0.2380	-13.5	0.963	0.9597	0.34	1.536	1.502	2.21
21	5.83	31.5	6.548	xx	4.025	xx	xx	7.1620	xx	xx	0.5141	xx	xx	0.9282	xx	xx	1.978	xx
22	7.77	31.5	6.548	6.13	6.017	1.84	7.7583	7.6060	1.96	0.3724	0.3878	-4.13	0.952	0.949	0.31	1.828	1.863	-1.91
23	9.71	31.5	6.548	7.96	8.01	-0.62	8.1052	8.1220	-0.20	0.3080	0.3299	-7.11	0.962	0.9593	0.28	1.75	1.747	0.17
24	11.64	31.5	6.548	9.79	9.993	-2.07	8.6566	8.7160	-0.68	0.2597	0.2970	-14.3	0.97	0.9659	0.42	1.641	1.633	0.48
25	13.58	31.5	6.548	11.62	11.98	-3.09	8.9111	9.4110	-5.60	0.2406	0.2760	-14.7	0.973	0.9706	0.24	1.575	1.517	3.68

Note: (xx) means the experimental data have not been reported.

Table 3

Model validation with experimental results for inlet feed flow rate of ($F_{b(0,y)}$ =2.33E-4 m³/s)

				Pb(outlet), (atm)			Cb(outlet)x10³ (kmol/m³)			Cp(av.)x10³ (kmol/m³)			Rej(av)			Fb(outlet)x10⁴ (m³/s)		
No	Pb(inlet), (atm)	Tb(inlet), (°C)	Cb(inlet) x10³ (kmol/m³)	Exp.	The.	%Error	Exp.	The.	%Error	Exp.	The.	%Error	Exp.	The.	%Error	Exp.	The.	%Error
1	5.83	32.5	0.819	4.39	3.92	10.7	0.9432	0.9127	3.24	0.0915	0.0887	3.06	0.903	0.9028	0.02	1.957	2.085	-6.54
2	7.77	32.5	0.819	6.23	5.916	5.04	1.0058	0.9740	3.16	0.0855	0.0723	15.4	0.915	0.9257	-1.16	1.86	1.955	-5.10
3	9.71	32.5	0.819	8.06	7.916	1.78	1.0600	1.0450	1.41	0.0742	0.0647	12.8	0.93	0.9381	-0.87	1.742	1.825	-4.76
4	11.64	32.5	0.819	9.9	9.907	-0.07	1.1246	1.1300	-0.47	0.0731	0.0605	17.2	0.935	0.9465	-1.22	1.639	1.694	-3.35
5	13.58	32.5	0.819	11.73	11.908	-1.51	1.1961	1.2280	-2.66	0.0622	0.0580	6.75	0.948	0.9527	-0.49	1.542	1.566	-1.55
6	5.83	31	1.637	4.34	3.91	9.90	1.8753	1.8113	3.41	0.1519	0.1730	-13.8	0.919	0.904	1.63	2.01	2.1	-4.47
7	7.77	31	1.637	6.19	5.899	4.70	1.9830	1.9280	2.77	0.1289	0.1390	-7.83	0.935	0.9274	0.81	1.894	1.9758	-4.31
8	9.71	31	1.637	8.02	7.905	1.43	2.0929	2.0620	1.48	0.1193	0.1240	-3.93	0.943	0.9397	0.34	1.794	1.848	-3.01
9	11.64	31	1.637	9.86	9.89	-0.30	2.2019	2.2170	-0.68	0.1123	0.1150	-2.40	0.949	0.9478	0.12	1.684	1.723	-2.31
10	13.58	31	1.637	11.68	11.88	-1.71	2.3617	2.4000	-1.62	0.1110	0.1103	0.63	0.953	0.954	-0.10	1.594	1.5988	-0.30
11	5.83	31	2.455	4.29	3.898	9.13	2.7734	2.7060	2.43	0.2302	0.2370	-2.95	0.917	0.9123	0.51	2.022	2.109	-4.30
12	7.77	31	2.455	6.14	5.894	4.00	2.9513	2.8750	2.58	0.2125	0.1874	11.8	0.928	0.9348	-0.73	1.907	1.986	-4.14
13	9.71	31	2.455	7.97	7.89	1.00	3.1000	3.0700	0.96	0.1736	0.1645	5.24	0.944	0.9464	-0.25	1.815	1.863	-2.64
14	11.64	31	2.455	9.81	9.876	-0.67	3.2800	3.2940	-0.42	0.1640	0.1515	7.62	0.95	0.954	-0.42	1.707	1.74	-1.93
15	13.58	31	2.455	11.64	11.88	-2.06	3.5022	3.5580	-1.59	0.1541	0.1435	6.87	0.956	0.9596	-0.37	1.591	1.618	-1.69
16	5.83	30	4.092	4.25	3.887	8.54	4.5546	4.4680	1.90	0.2915	0.2770	4.97	0.936	0.938	-0.21	2.072	2.129	-2.75
17	7.77	30	4.092	6.1	5.88	3.60	4.7964	4.7240	1.51	0.2734	0.3100	-13.3	0.943	0.9343	0.92	1.974	2.015	-2.07
18	9.71	30	4.092	7.92	7.87	0.63	4.9938	5.0220	-0.56	0.2447	0.2690	-9.93	0.951	0.9464	0.48	1.887	1.897	-0.52
19	11.64	30	4.092	9.76	9.85	-0.92	5.1790	5.3610	-3.51	0.2227	0.2460	-10.4	0.957	0.9541	0.30	1.805	1.783	1.21
20	13.58	30	4.092	11.59	11.85	-2.24	5.4361	5.7550	-5.86	0.1957	0.2310	-18.0	0.964	0.9597	0.44	1.722	1.664	3.36
21	5.83	31.5	6.548	xx	3.88	xx	xx	7.1040	xx	xx	0.5190	xx	xx	0.9269	xx	xx	2.144	xx
22	7.77	31.5	6.548	6.05	5.873	2.92	7.5553	7.5100	0.59	0.3551	0.3844	-8.25	0.953	0.9488	0.44	1.987	2.029	-2.11
23	9.71	31.5	6.548	7.88	7.87	0.12	7.8131	7.9977	-2.36	0.2969	0.3240	-9.12	0.962	0.9593	0.28	1.902	1.913	-0.57
24	11.64	31.5	6.548	9.72	9.85	-1.33	8.1806	8.5100	-4.02	0.2536	0.2901	-14.3	0.969	0.9659	0.31	1.815	1.798	0.93
25	13.58	31.5	6.548	11.54	11.84	-2.59	8.6740	9.1260	-5.21	0.2342	0.2680	-14.4	0.973	0.9705	0.25	1.734	1.681	3.05

Note: (xx) means the experimental data have not been reported

Table 4

Model validation with experimental results for inlet feed flow rate of ($F_{b(0,y)}$ =2.583E-4 m³/s)

				Pb(outlet), (atm)		%Error	Cb(outlet)x10³ (kmol/m³)		%Error	Cp(av.)x10³ (kmol/m³)		%Error	Rej(av)		%Error	Fb(outlet)x10⁴ (m³/s)		%Error
No	Pb (inlet) (atm)	Tb(inlet) (°C)	Cb(inlet) x10³ (kmol/m³)	Exp.	The.		Exp.	The.		Exp.	The.		Exp.	The.		Exp.	The.	
1	5.83	32.5	0.819	4.27	3.69	13.5	0.9290	0.8997	3.15	0.0864	0.08958	-3.68	0.907	0.9004	0.72	2.199	2.345	-6.63
2	7.77	32.5	0.819	6.11	5.69	6.87	0.9975	0.9533	4.43	0.0798	0.07102	11.0	0.92	0.9255	-0.59	2.075	2.21	-6.50
3	9.71	32.5	0.819	7.94	7.69	3.14	1.0610	1.0160	4.24	0.0626	0.06267	-0.11	0.941	0.9383	0.28	1.953	2.08	-6.50
4	11.64	32.5	0.819	9.78	9.67	1.12	1.1160	1.0840	2.86	0.0558	0.0582	-4.30	0.95	0.9462	0.40	1.838	1.955	-6.36
5	13.58	32.5	0.819	11.61	11.68	-0.60	1.2073	1.1783	2.40	0.0495	0.0551	-11.3	0.959	0.9531	0.61	1.72	1.807	-5.05
6	5.83	31	1.637	4.22	3.68	12.7	1.8481	1.7880	3.25	0.1460	0.1750	-19.8	0.921	0.9016	2.10	2.261	2.359	-4.33
7	7.77	31	1.637	6.07	5.68	6.42	1.9523	1.8890	3.24	0.1230	0.1370	-11.3	0.937	0.9271	1.05	2.148	2.23	-3.81
8	9.71	31	1.637	7.89	7.67	2.78	2.0456	2.0050	1.98	0.1166	0.1210	-3.77	0.943	0.9396	0.36	2.042	2.107	-3.18
9	11.64	31	1.637	9.73	9.67	0.61	2.1461	2.1360	0.47	0.1116	0.1149	-2.95	0.948	0.9478	0.02	1.947	1.982	-1.79
10	13.58	31	1.637	11.56	11.66	-0.86	2.2204	2.2880	-3.04	0.1088	0.1056	2.94	0.951	0.9538	-0.29	1.85	1.855	-0.27
11	5.83	31	2.455	4.17	3.675	11.8	2.7457	2.6720	2.68	0.2279	0.2400	-5.30	0.917	0.91	0.76	2.29	2.368	-3.40
12	7.77	31	2.455	6.02	5.671	5.79	2.8985	2.8200	2.71	0.2000	0.1847	7.65	0.931	0.9345	-0.37	2.173	2.245	-3.31
13	9.71	31	2.455	7.85	7.668	2.31	2.9821	2.9880	-0.19	0.1670	0.1602	4.07	0.944	0.9464	-0.25	2.08	2.121	-1.97
14	11.64	31	2.455	9.66	9.654	0.06	3.1659	3.1790	-0.41	0.1488	0.1463	1.68	0.953	0.9539	-0.09	1.97	1.997	-1.37
15	13.58	31	2.455	11.51	11.65	-1.21	3.3142	3.3990	-2.55	0.1392	0.1376	1.14	0.958	0.9595	-0.15	1.868	1.874	-0.32
16	5.83	29	4.092	xx	3.66	xx	xx	4.4080	xx	xx	0.3163	xx	xx	0.9282	xx	xxx	2.393	xx
17	7.77	29	4.092	xx	5.65	xx	xx	4.6300	xx	xx	0.2320	xx	xx	0.9498	xx	xx	2.278	xx
18	9.71	29	4.092	7.8	7.65	1.92	4.9000	4.8820	0.36	0.2303	0.1981	13.9	0.953	0.9594	-0.67	2.113	2.162	-2.31
19	11.64	29	4.092	9.61	9.63	-0.20	5.0476	5.1640	-2.30	0.2120	0.1803	14.9	0.958	0.965	-0.73	2.07	2.047	1.11
20	13.58	29	4.092	11.47	11.62	-1.30	5.3657	5.4860	-2.24	0.1878	0.1698	9.58	0.965	0.969	-0.41	1.972	1.93	2.12
21	5.83	31.5	6.548	4.08	3.66	10.2	7.1666	7.0360	1.82	0.3870	0.3810	1.55	0.946	0.9458	0.02	2.337	2.401	-2.73
22	7.77	31.5	6.548	5.93	5.65	4.72	7.5021	7.3880	1.52	0.3451	0.3812	-10.4	0.954	0.9483	0.59	2.253	2.287	-1.50
23	9.71	31.5	6.548	7.75	7.64	1.41	7.8270	7.7960	0.39	0.2896	0.3172	-9.53	0.963	0.9593	0.38	2.17	2.1703	-0.01
24	11.64	31.5	6.548	9.57	9.637	-0.70	8.0064	8.2550	-3.10	0.2482	0.2810	-13.2	0.969	0.9658	0.33	2.09	2.053	1.77
25	13.58	31.5	6.548	11.42	11.62	-1.75	8.5037	8.7780	-3.22	0.2296	0.2589	-12.7	0.973	0.9705	0.25	2.011	1.936	3.72

Note: (xx) means the experimental data have not been reported

Generally, the predicted values of the theoretical model are in a good agreement with the experimental ones over the ranges of pressures, feed flow rates and concentrations. Figs. 2 and 3 show the agreement between the experimental and predicted values of outlet feed concentration and solute rejection for the whole data within 5% error and 2.1% error respectively. While the model is able to predict the permeate concentration within a maximum of 15% error (Tables 2 – 4) and less than 4% error for about 76% of outlet feed flow rate readings. Finally, 79% of outlet feed pressure readings are within 4% error as well. The model is then used for further simulation as reported in the next section.

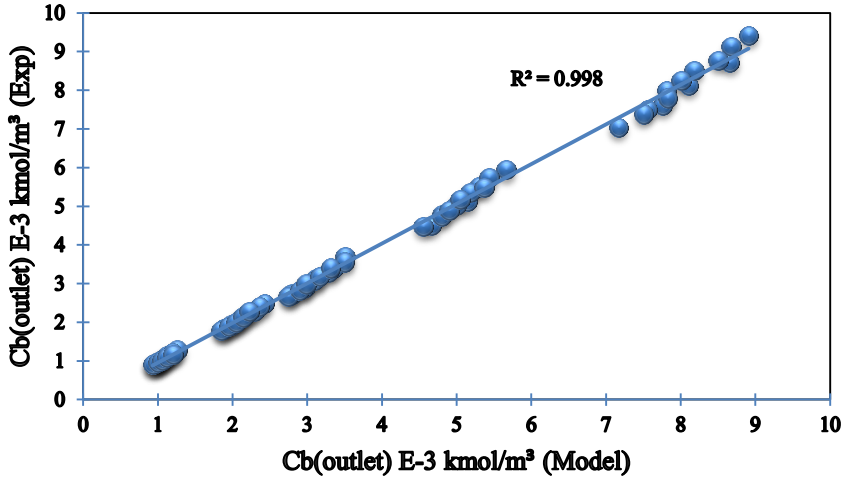

Fig. 2. Comparison of experimental and model prediction of outlet brine concentration

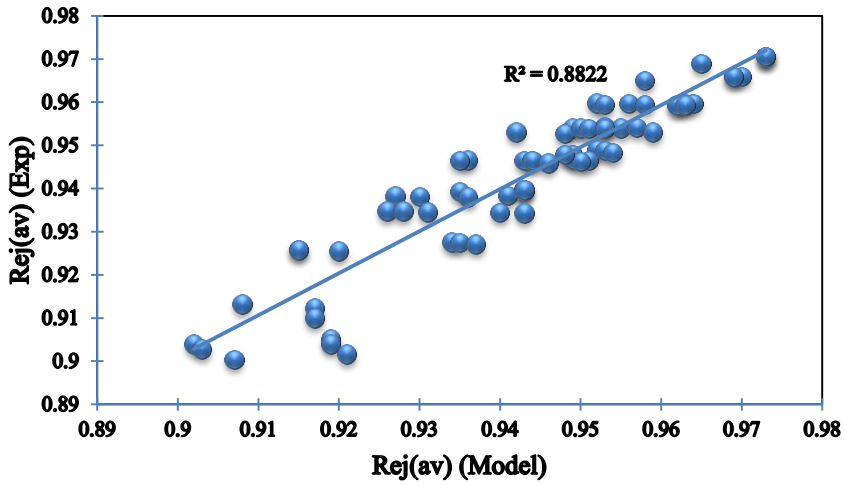

Fig. 3. Comparison of experimental and model prediction of solute rejection

4.2.2 The effects of processing parameters on performances of RO module

The two-dimensional results plotted in Figs. 4 and 5 show the output data of using the model with a rich insight into the steady state feed flow rate and pressure in two dimensions throughout the membrane sheet. The feed flow rate decreases quite quickly as water passing through the membrane with a rapid increase in the osmotic pressure due to an increase in solute concentration. It was also noted that the feed pressure drops off at the end of the membrane length by increasing pressure loss due to friction in wall membrane.

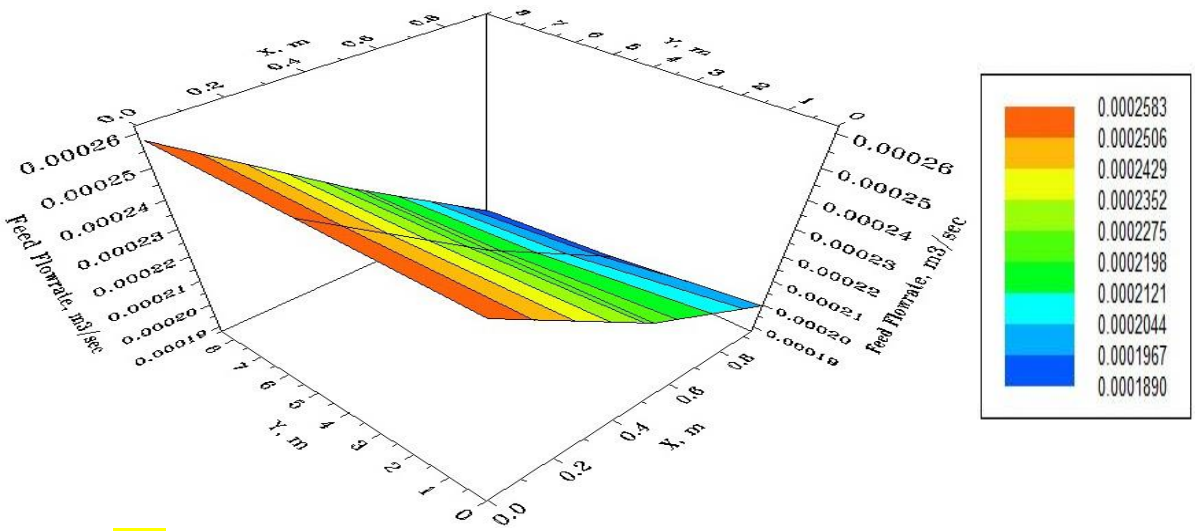

Fig. 4. Feed flow rate in the two dimensions at inlet conditions (2.583E-4 m^3/s, 6.548E-3 $kmol/m^3$, 13.58 atm and 31.5 °C

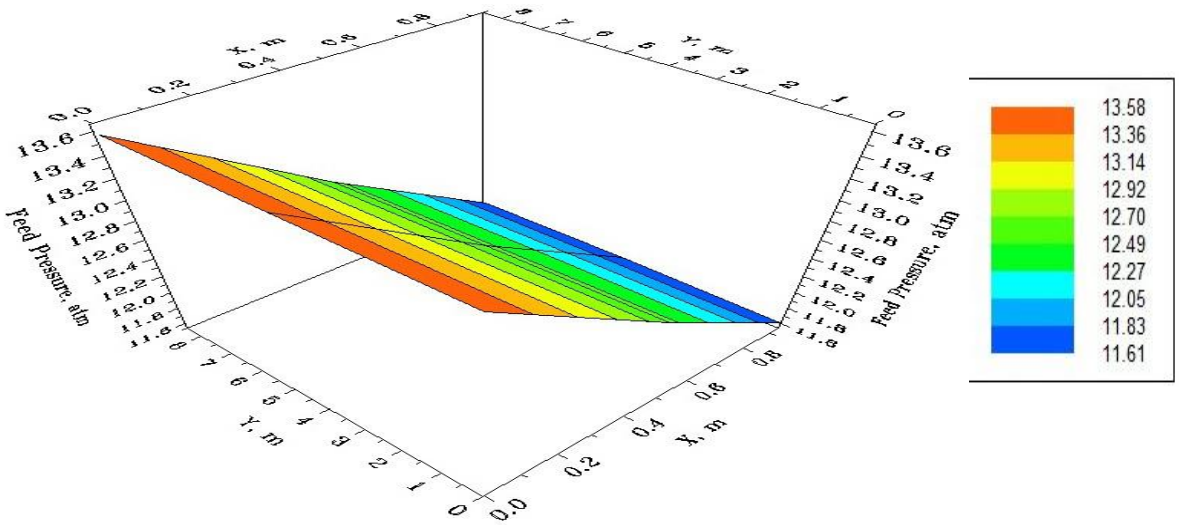

Fig. 5. Feed pressure in the two dimensions at inlet conditions (2.583E-4 m³/s, 6.548E-3 kmol/m³, 13.58 atm and 31.5 °C

Fig. 6 clearly shows the spatial progress of feed concentration in two dimensions in the feed channel due to retained solute along the membrane wall. This results in increasing the concentration polarization and osmotic pressure by building up the solute on the membrane and causing a reduction in water flux by reducing the pressure driving force as can be shown in Eq. (1).

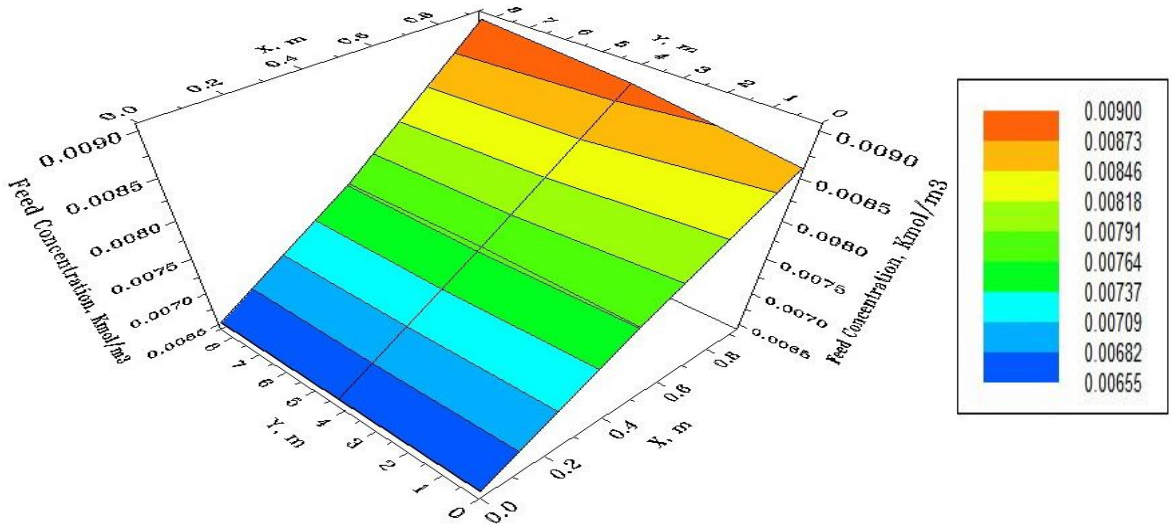

Fig. 6. Feed concentration in the two dimensions at inlet conditions (2.583E-4 m³/s, 6.548E-3 kmol/m³, 13.58 atm and 31.5 °C

Fig. 7 depicts the spatial behaviour of water flux in two dimensions. It is worth mentioning that the water flux increases with *y* coordinates progress along the *x* dimension. This might be attributed to somehow higher registered values of applied pressure at the outlet edge of the membrane width (Fig. 5) in comparison to the inlet edge of the membrane width due to lower registered feed flow rate (Fig. 4) and friction.

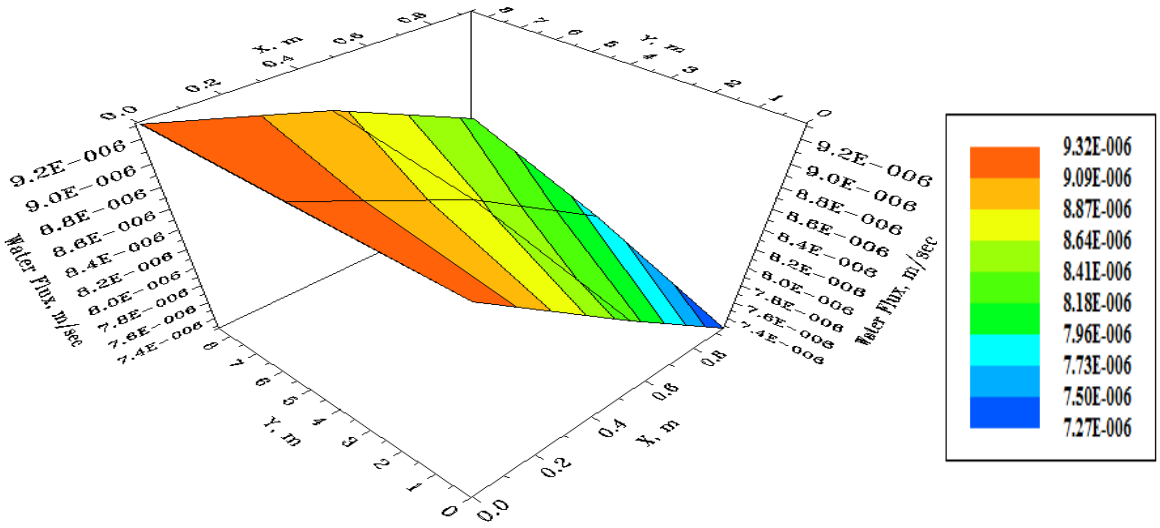

Fig. 7. Water flux in the two dimensions at inlet conditions (2.583E-4 m^3/s, 6.548E-3 $kmol/m^3$, 13.58 atm and 31.5 °C

In addition, the wall membrane concentration increases along the membrane due to the impact of solute rejection on the wall membrane (Fig. 8).

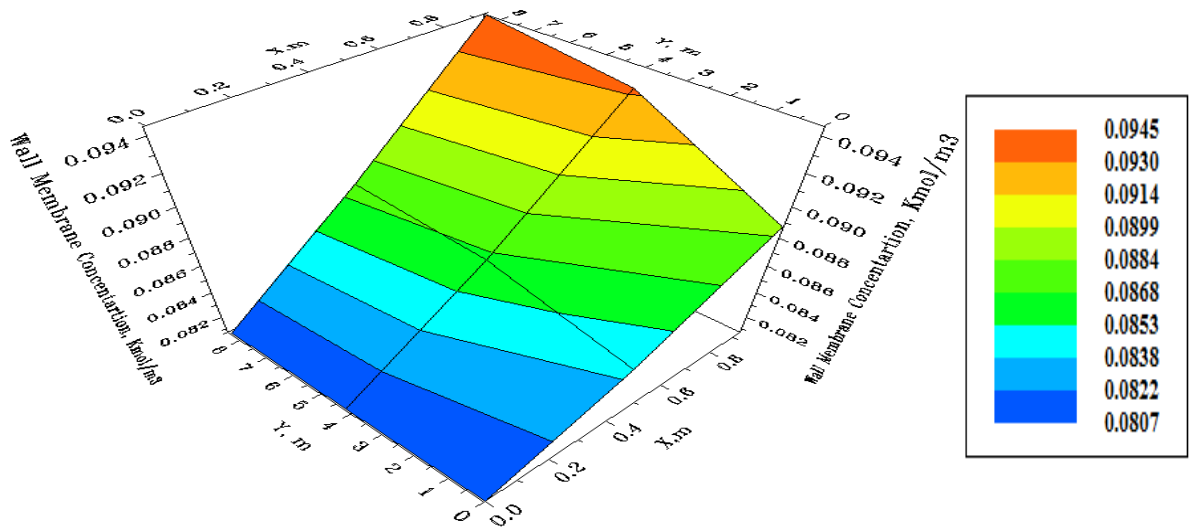

Fig. 8. Wall membrane concentration in the two dimensions at inlet conditions (2.583E-4 m³/s, 6.548E-3 kmol/m³, 13.58 atm and 31.5 °C

Here, the model is used to simulate the process, see the sensitivity of the model to different parameters of the process, and take an overview of the membrane performance under the impact of varying the process parameters, such as, inlet feed flow rate, inlet feed concentration, inlet feed pressure and inlet feed temperature. Then, solute rejection and % total water recovery can be recorded (Figs. 9 to 16).

Fig. 9 shows the response of solute rejection for the variation in both inlet feed pressure from (5.83 to 13.58 atm) and inlet feed concentration from (0.819E-3 to 6.548E-3 kmol/m³) with constant values of the inlet feed flow rate and temperature (2.583E-4 m³/s and 31 ºC) respectively.

It will be noted that the dimethylphenol rejection varies between 88 and 96.8 %. Also, the solute rejection increases as a result to increase in the inlet feed pressure and concentration. This is due to increase in water flux by increasing inlet feed pressure, which reduces solute concentration in the permeate channel. Also, the membrane rejection intensity increases as a result to increase in the inlet feed concentration.

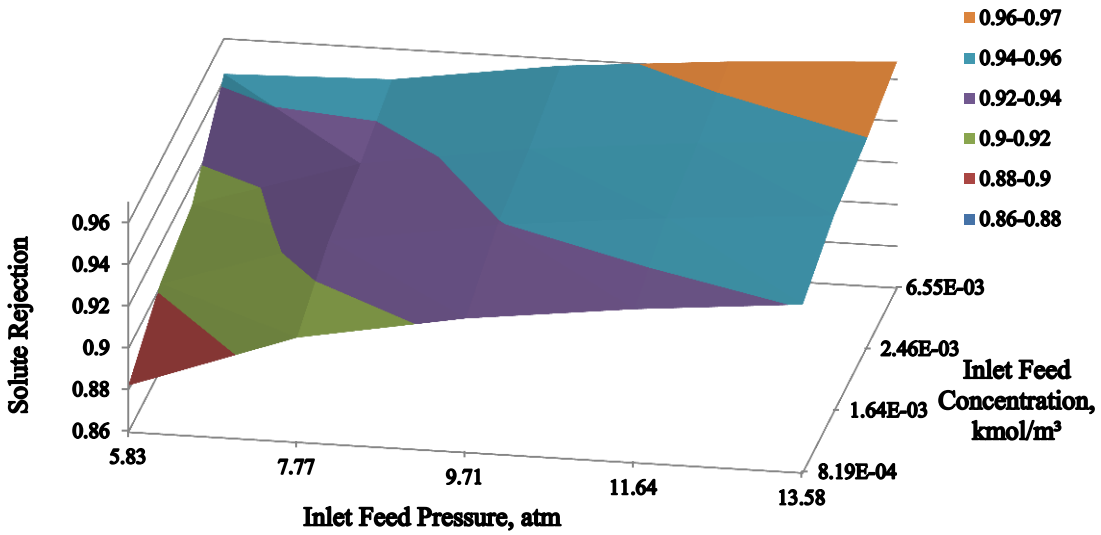

Fig. 9. Impact of variation in inlet feed pressure and concentration on solute rejection at fixed inlet feed flow rate and temperature (2.583E-4 m³/s and 31 ºC)

Fig. 10 depicts the response of solute rejection for the variation in both inlet feed flow rate from 2.166E-4 to 2.583E-4 m³/s, and inlet feed pressure from 5.83 to 13.58 atm with constant values of high inlet feed concentration and temperature (6.548E-3 kmol/m³ and 31 ºC) respectively.

It is noted that at high concentrations and high pressures conditions, increasing inlet feed flow rate has a comparable impact on the solute rejection in comparison to using high concentrations and low pressures conditions. The reason for this can be explained as follows.

At low pressure conditions, increasing inlet feed flow rate results in decreasing the concentration polarization, which reduces the solute concentration along the wall membrane and the solute flux through the membrane. Then, this will decrease the permeate solute concentration and increase the solute rejection. However, at high pressure conditions, it seems that there is a conflict between the operating variables. Firstly, high pressure increases water flux due to decrease in the osmotic pressure. However, the water flux somewhat decreases by increasing the friction with the membrane wall. This might be explained a lower impact of increasing inlet feed flow rate on solute rejection response at high inlet feed concentrations.

On the other hand, using lower inlet feed concentration, the experimental data (Tables 2 – 4) show somehow an increase in average solute rejection by increasing the inlet feed flow rate. This is due to the absence of concentration polarization impact at lower feed concentrations, which increases the mass transfer coefficient and the total permeated water. Furthermore, increasing the applied pressure results in reducing the concentration of permeate water and at the same time increasing the solute rejection due to increase in water flux.

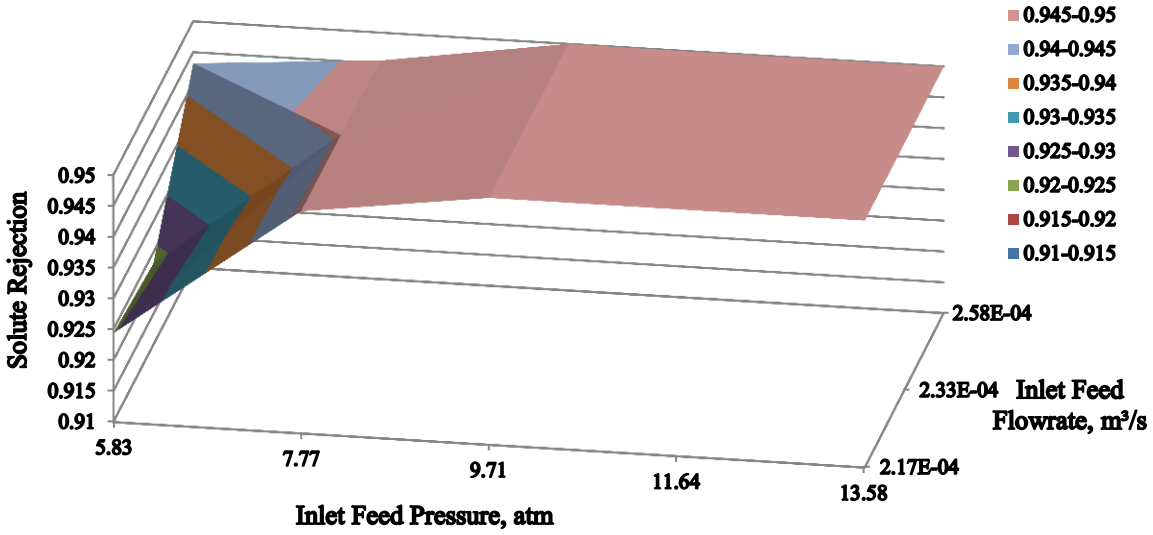

Fig. 10. Impact of variation in inlet feed pressure and flow rate on solute rejection at fixed inlet feed concentration and temperature (6.548E-3 kmol/ m³ and 31 ºC)

Fig. 11 clearly shows the response of solute rejection for the variation in inlet feed concentration from 0.819E-3 to 6.548E-3 kmol/m³, and inlet feed flow rate from 2.166E-4 to 2.583E-4 m³/s with constant values of inlet feed pressure and temperature (13.58 atm and 31 ºC) respectively.

It is clear that the impact of variation in inlet feed concentration on solute rejection is comparable to the inlet feed flow rate in the case of using high inlet feed pressure conditions (Fig. 11). The solute rejection increases as a result to increase in the inlet feed concentration and this may be due to increase in the membrane solute isolation intensity. While, increasing

inlet feed flow rate at high operating pressure results in a little increase in solute rejection for all the operating concentrations (Table 2 – 4).

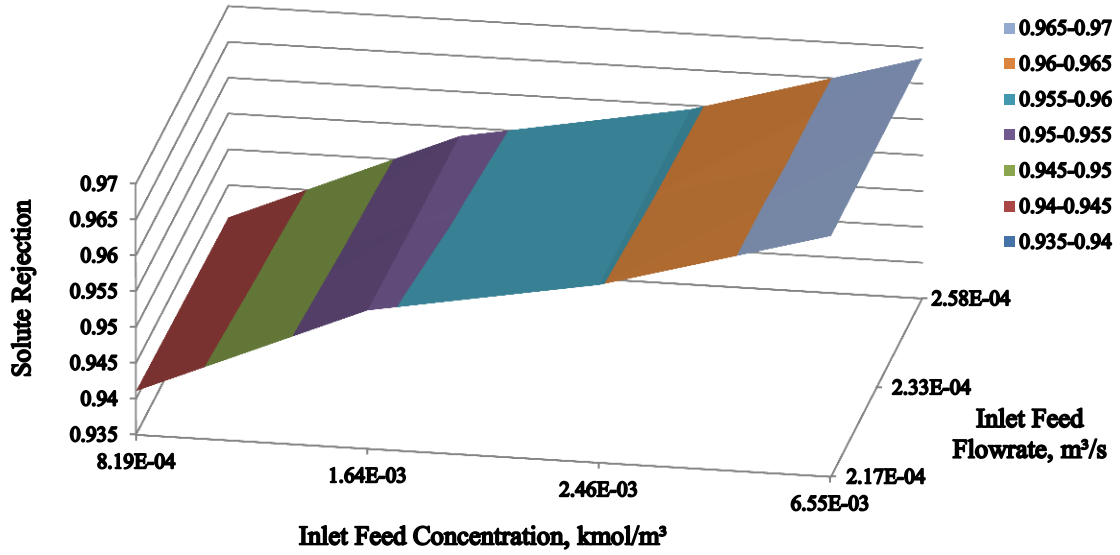

Fig. 11. Impact of variation in inlet feed concentration and flow rate on solute rejection at fixed inlet feed pressure and temperature (13.58 atm and 31 ºC)

Also, it is easy to notice that the temperature has a significant impact on the solute rejection (Fig. 12). Increasing the operating temperature results in decreasing the viscosity of brine and increasing water flux and reducing the concentration at the permeate channel.

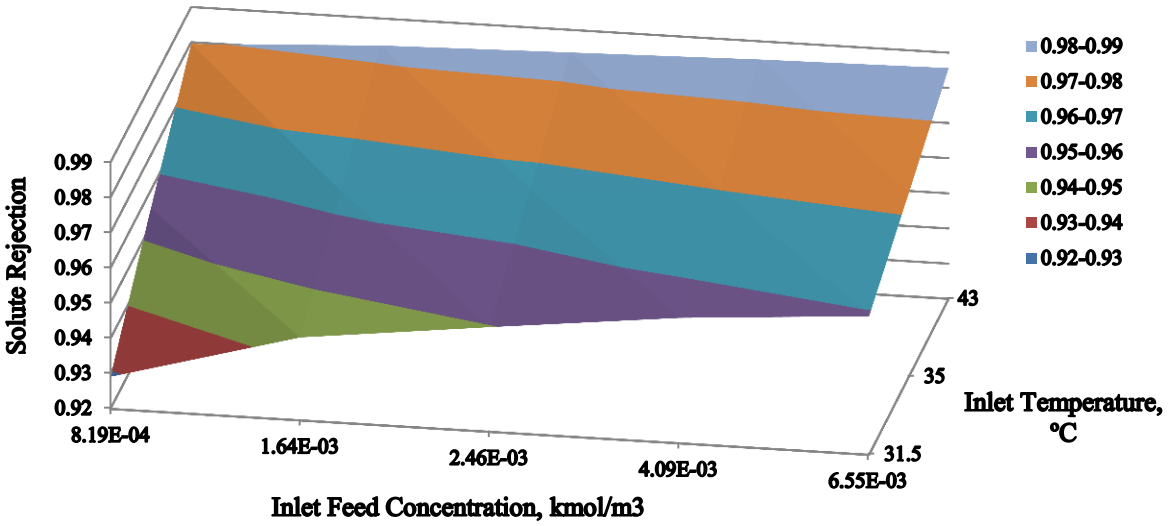

Fig. 12. Impact of variation in inlet feed concentration and temperature on solute rejection at fixed inlet feed pressure and flow rate (9.71 atm and 2.166E-4 m³/s)

Figs. 13 to 16 show the output plotting of % total water recovery for the variation in inlet feed flow rate, inlet feed concentration, inlet feed pressure and inlet feed temperature respectively. Fig. 13 shows an increasing % total water recovery as a result of the increase in the operating pressure that lifts the quantity of water flux. While the % total water recovery decreases as a result of the increase in operating concentration due to the reduction of water flux caused by increasing osmotic pressure that reduces the driving force $(\Delta P_b - \Delta\pi)$ of water flux.

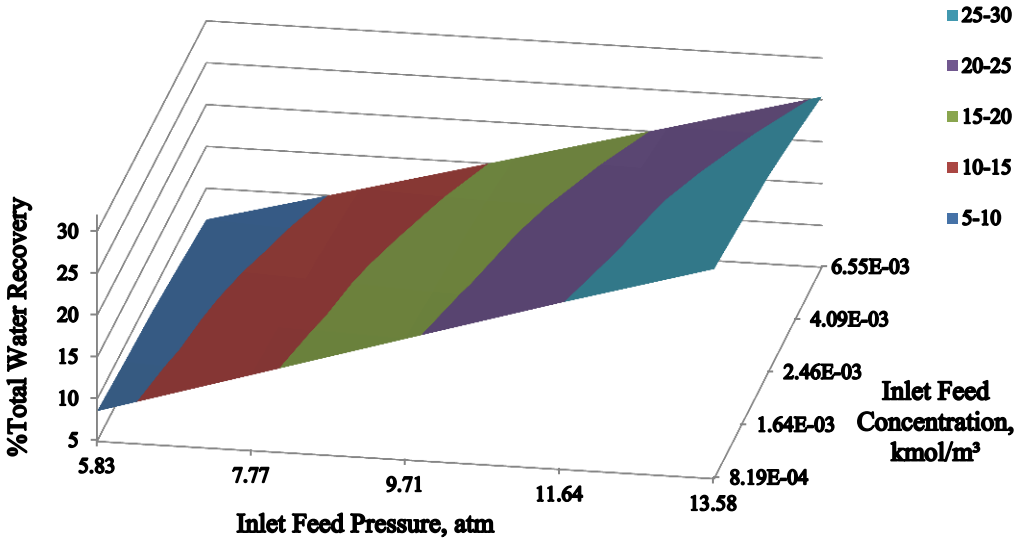

Fig. 13. Impact of variation in inlet feed pressure and concentration on %total water recovery at fixed inlet feed flow rate and temperature (2.583E-4 m³/s and 31 ºC)

Figs. 14 and 15 show a reduction of % total water recovery as a result of the increase in the inlet feed flow rate in spite of the gain of osmotic pressure reduction. It seems that, increasing inlet feed flow rate leads to an increase in the frictional pressure drop along the membrane that creates a low driving force for the flow of fresh water in addition to a decrease in the residence time of feed inside the unit.

Also, % total water recovery decreases as a result of the increase in operating concentration. This is due to increase in the osmotic pressure, which in turn reduces water flux.

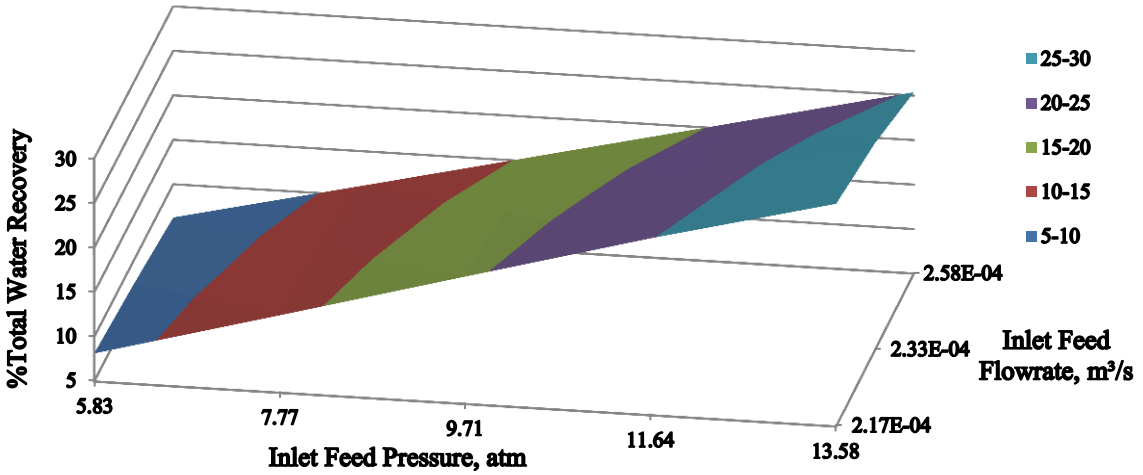

Fig. 14. Model simulation of %total water recovery at varying inlet feed flow rate and inlet feed pressure at fixed inlet feed concentration temperature (6.548E-3 kmol/m³ and 31 ºC)

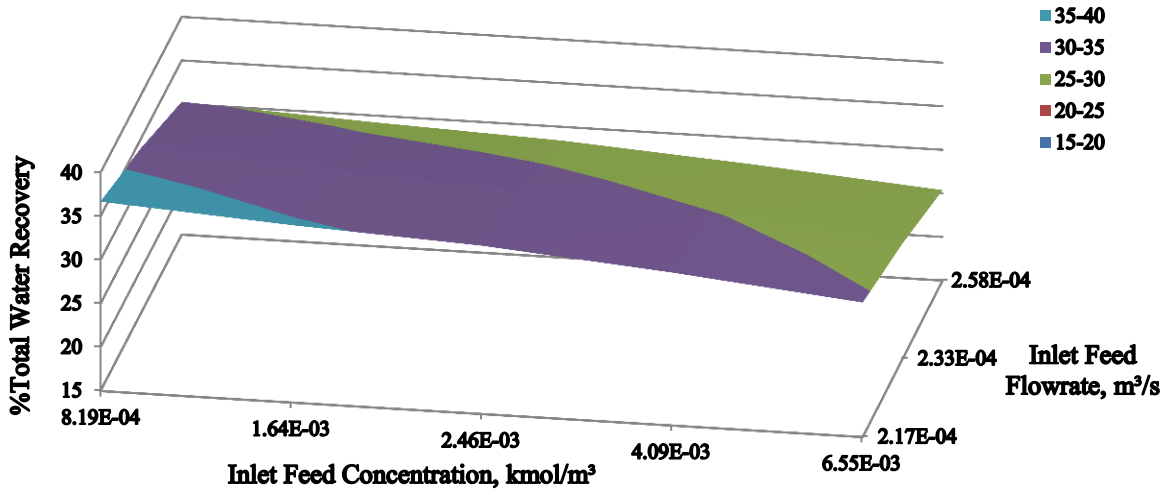

Fig. 15. Impact of variation in inlet feed concentration and flow rate on %total water recovery at fixed inlet feed pressure and temperature (13.58 atm and 31 ºC)

Lastly, increasing operating temperature has a significant impact on % total water recovery by increasing the quantity of water flux, as depicted in Fig. 16.

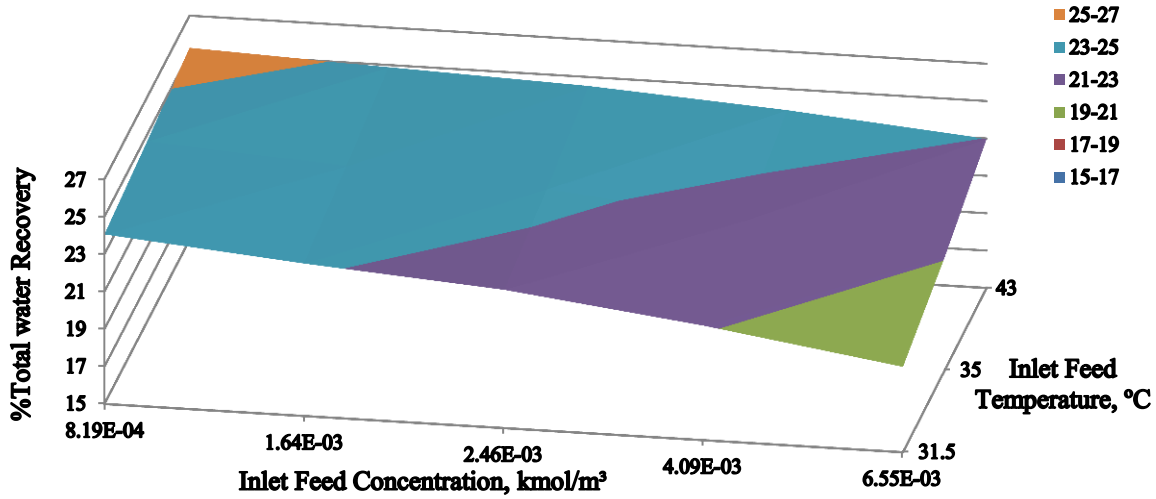

Fig. 16. Impact of variation in inlet feed concentration and temperature on %total water recovery at fixed inlet feed pressure and flow rate (9.71 atm and 2.166E-4 m^3/s)

5. Conclusions

A two-dimensional mathematical model applicable for dilute aqueous solution in a spiral-wound RO system has been developed and validated with a wastewater simulation study. The model can be used to predict the flow rate, concentration, pressure and temperature in each point along the two sides of the membrane length and width. Furthermore, this model facilitates the estimation of the behavior of water flux, solute flux and solute concentration on the wall of the membrane. A number of explicit differential equations have been developed for estimating the operating parameters with spatial dimensions. The model looks at the impact of concentration, pressure and temperature on the physical properties of the solution by considering varied mass transfer coefficient and concentration polarization. The predictions of this model have been compared to the experimental data from the literature at steady state which show a good agreement with an accepted relative error for most operating parameters.

The model is developed in *gPROMS* in a way that it can be used for multi-component system, which will be considered in future work. In particular, the study shows that

increasing feed flow has little impact on solute rejection at high concentrations and pressures, while the membrane rejection intensity increased with increasing inlet feed concentration.

Nomenclature

A_m : Area of the membrane (m^2)

A_w : Solvent transport coefficient (m/atm s).

b : Feed and permeate channels friction parameter (atm s/m^4).

B_s : Solute transport coefficient (m/sec).

C_b : Brine solute concentration in the feed channel (kmol/m^3).

C_p : Permeate solute concentration in the permeate channel (kmol/m^3).

C_m : Dimensionless solute concentration.

C_w : Solute concentration at the membrane wall (kmol/m^3).

D_b : Diffusivity of feed (m^2/s).

D_p : Diffusivity of permeate (m^2/s).

d_{ep} : Equivalent diameter of feed channel (m).

d_{ef} : Equivalent diameter of permeate channel (m).

F_b : Feed flow rate (m^3/s).

F_p : Permeate flow rate (m^3/s).

F_s : Solute molar flux in x-axis (kmol/m^2 s).

J_s : Solute molar flux through the membrane (kmol/m^2 s).

J_w : Water flux (m/s).

k : Mass transfer coefficient (m/s).

L : Length of the membrane (m).

M_{wb} : Molecular weight of brine water (kg/kmol).

P_b : Feed pressure (atm).

P_p : Permeate pressure (atm).

R : Gas low constant $\left(\mathrm{R} = 0.082\,\frac{\mathrm{atm\ m^3}}{\mathrm{^\circ K\ kmol}}\right)$.

Rec : Water recovery coefficient (dimensionless).

$Rec_{(Total)}$: Total water recovery for the whole unit (dimensionless).

Rej : Solute rejection coefficient (dimensionless).

$Rej_{(av)}$: Average solute rejection coefficient (dimensionless).

Re_b : Feed Reynolds number (dimensionless).

Re_p : Permeate Reynolds number (dimensionless).

T_b : Feed temperature (°C).

t_f : Feed spacer thickness (mm).

T_p : Permeate temperature (°C).

t_p : Permeate spacer thickness (mm).

W : Width of the membrane (m).

Δx : Length of sub-section (m).

μ_b : Feed viscosity (kg/m s).

μ_p : Permeate viscosity (kg/m s).

ρ_b : Feed density (kg/m³).

ρ_p : Permeate density (kg/m³).

ρ_w : Molal density of water (55.56 kmol/m³).

References

Ahmad A. L., Chong M. F. and Bhatia S. 2007. Mathematical modeling of multiple solutes system for reverse osmosis process in palm oil mill effluent (POME) treatment. The Chemical Engineering Journal, 132, 183-193.

Álrez S., Riera F. A., Álvarez R. and Coca J. 2002. Concentration of Apple Juice by Reverse Osmosis at Laboratory and Pilot-Plant Scales. Industrial & Engineering Chemistry Research, 41, 6156-6164.

Amar N. B., Kechaou N., Palmeri J., Deratani A. and Sghaier A. 2009. Comparison of tertiary treatment by nanofiltration and reverse osmosis for water reuse in denim textile industry. Journal of Hazardous Materials, 170, 111-117.

Avlonits S., Hanbury W. T. and Boudinar M. B. 1991. Spiral wound modules performance. An analytical solution - part I. Desalination, 81**,** 191-208.

Avlonits S. A., Pappas M. and Moutesidis K. 2007. A unified model for the detailed investigation of membrane modules and RO plants performance. Desalination, 203**,** 218-228.

Bhattacharya P., Roy A., Sarkar S., Ghosh S., Majumdar S., Chakraborty S., Mandal S., Mukhopadhyay A. and Bandyopadhyay S. 2013. Combination technology of ceramic microfiltration and reverse osmosis for tannery wastewater recovery. Water Resources and Industry, 3, 48-62.

Boudinar M. B., Hanbury W. T. and Avlonits S. 1992. Numerical simulation and optimisation of spiral-wound modules. Desalination, 86**,** 273-290.

Chew C. M., Aroua M. K., Hussain M. A. and Ismail W. M. Z. W. 2016. Evaluation of ultrafiltration and conventional water treatment systems for sustainable development: an industrial scale case study. Journal of Cleaner Production 112, 3152-3163

Evangelista F. 1988. An improved analytical method for the design of spiral-wound modules. The Chemical Engineering Journal, 38**,** 33-40.

Fujioka T., Khan S. J., Mcdonald J. A., Roux A., Poussade,Y., Drewes J. E. and Nghiem L. D. 2014. Modelling the rejection of N-nitrosamines by a spiral-wound reverse osmosis system: Mathematical model development and validation. Journal of Membrane Science, 454, 212-219.

Geraldes V., Escórcio Pereira N. and Norberta de Pinho M. 2005. Simulation and Optimization of Medium-Sized Seawater Reverse Osmosis Processes with Spiral-Wound Modules. Industrial and Engineering Chemistry Research, 44(6), 1897-1905.

Gupta S. K. 1985. Analytical design equations for reverse osmosis systems. Ind. Eng. Chem. Process Des. Dev., 24, 1240-1244.

Kaghazchi T., Mehri M., Takht Ravanchi M. and Kargari A. 2010. A mathematical modeling of two industrial seawater desalination plants in the persian gulf region. Desalination, 252, 135-142.

Karabelas A. J., Koutsou C. P. and Kostoglou M. 2014. The effect of spiral wound membrane element design characteristics on its performance in steady state desalination — A parametric study. Desalination, 332**,** 76-90.

Koroneos C., Dompros A. and Roumbas G. 2007. Renewable energy driven desalination systems modelling. Journal of Cleaner Production, 15**,** 449-464.

Koyuncu I., Topacik M. T. and Ates A. 2000. Application of low pressure nanofiltration membranes for the recovery and reuse of dairy industry effluents. Water Sci. Technol., 41(l) 213-221.

Lee S. and Lueptow R. M. 2001. Rotating reverse osmosis: a dynamic model for flux and rejection. Journal of Membrane Science, 192**,** 129-143.

Lonsdale H. K., Merten U. and Riley R. L. 1965. Transport properties of cellulose acetate osmotic membranes. Journal of Applied Polymer Science, 9**,** 1341-1362.

Mane P. P., Park P. K., Hyung H., Brown J. C. and Kim J.H. 2009. Modeling boron rejection in pilot- and full-scale reverse osmosis desalination processes. Journal of Membrane Science, 338**,** 119-127.

Mitra-Gholami R. M., Kalantary R. R., Sabzali A. and Gatei F. 2012. Performance evaluation of reverse osmosis technology for selected antibotics removal from synthetic pharmaceutical wastewater. Iranian Journal of Environmental Health Sciences & Engineering, 9:19.

Oh H., Hwang T. and Lrr S. 2009. A simplified model of RO systems for seawater desalination. Desalination, 238, 128-139.

Process System Enterprise Ltd., (2001). gPROMS Introductory User Guide. London: Process System Enterprise Ltd.

Rautenbach R. and Dahm W. 1987. Design and optimization of spiral-wound and hollow fiber RO-modules. Desalination, 65**,** 259-275.

Sagne C. Fargues C., Broyart B., Lameloise M. and Decloux M. 2009. Modeling permeation of volatile organic molecules through reverse osmosis spiral-wound membranes. Journal of Membrane Science, 330(1–2), 40-50.

Sassi K.M. and Mujtaba I.M. 2011. Optimal design and operation of reverse osmosis desalination process with membrane fouling, The Chemical Engineering Journal, 171, 582–593.

Senthilmurugan S., Ahluwalia A. and Gupta S. K. 2005. Modeling of a spiral-wound module and estimation of model parameters using numerical techniques. Desalination, 173**,** 269-286.

Spiegler K. S. and Kedem O. 1966. Thermodynamics of hyperfiltration (reverse osmosis): criteria for efficient membranes. Desalination, 1, 311-326.

Srinivasan G., Sundaramoorthy S. and Murthy D. V. R. 2011. Validation of an analytical model for spiral wound reverse osmosis membrane module using experimental data on the removal of dimethylphenol. Desalination, 281**,** 199-208.

Sundaramoorthy S., Srinivasan G. and Murthy D. V. R. 2011a. An analytical model for spiral wound reverse osmosis membrane modules: Part I — Model development and parameter estimation. Desalination, 280**,** 403-411.

Sundaramoorthy S., Srinivasan G. and Murthy D. V. R. 2011b. An analytical model for spiral wound reverse osmosis membrane modules: Part II — Experimental validation. Desalination, 277**,** 257-264.

Taniguchi Y. 1978. An analysis of reverse osmosis characteristics of ROGA spiral-wound modules. Desalination, 25**,** 71-8.